AGU PUBLICATIONS

Geophysical Research Letters

RESEARCH LETTER
10.1002/2014GL061679

Key Points:
- New ground-based technique
- Pump-induced suprathermal electrons cause anomalous resistivity
- Anomalous electric field hinders ion outflow

Correspondence to:
M. J. Kosch,
mkosch@sansa.org.za

Citation:
Kosch, M. J., H. Vickers, Y. Ogawa, A. Senior, and N. Blagoveshchenskaya (2014), First observation of the anomalous electric field in the topside ionosphere by ionospheric modification over EISCAT, *Geophys. Res. Lett.*, *41*, 7427–7435, doi:10.1002/2014GL061679.

Received 1 SEP 2014
Accepted 21 OCT 2014
Accepted article online 24 OCT 2014
Published online 12 NOV 2014

The copyright line for this article was changed on 3 AUG 2015 after original online publication.

First observation of the anomalous electric field in the topside ionosphere by ionospheric modification over EISCAT

M. J. Kosch[1,2,3], H. Vickers[4], Y. Ogawa[1,5], A. Senior[3], and N. Blagoveshchenskaya[6]

[1]National Institute of Polar Research, Tokyo, Japan, [2]South African National Space Agency, Hermanus, South Africa, [3]Physics Department, Lancaster University, Lancaster, UK, [4]Institute for Physics and Technology, University of Tromsø, Tromsø, Norway, [5]Department of Polar Science, School of Multidisciplinary Sciences, Graduate University for Advanced Studies, Tokyo, Japan, [6]Arctic and Antarctic Research Institute, St. Petersburg, Russia

Abstract We have developed an active ground-based technique to estimate the steady state field-aligned anomalous electric field (E^*) in the topside ionosphere, up to ~600 km, using the European Incoherent Scatter (EISCAT) ionospheric modification facility and UHF incoherent scatter radar. When pumping the ionosphere with high-power high-frequency radio waves, the *F* region electron temperature is significantly raised, increasing the plasma pressure gradient in the topside ionosphere, resulting in ion upflow along the magnetic field line. We estimate E^* using a modified ion momentum equation and the Mass Spectrometer Incoherent Scatter model. From an experiment on 23 October 2013, E^* points downward with an average amplitude of ~1.6 μV/m, becoming weaker at higher altitudes. The mechanism for anomalous resistivity is thought to be low-frequency ion acoustic waves generated by the pump-induced flux of suprathermal electrons. These high-energy electrons are produced near the pump wave reflection altitude by plasma resonance and also result in observed artificially induced optical emissions.

1. Introduction

Anomalous resistivity in space plasmas and the ionosphere is a long-standing topic of study. The key to obtaining anomalous field-aligned resistance is the presence of low-frequency plasma density fluctuations (e.g., ion acoustic waves), which oscillating electrostatic field can effectively scatter drifting electrons due to their low mass [*Papadopoulos*, 1977]. Broadband extremely low frequency (BB-ELF, ~30–3000 Hz) ion waves have been observed in the topside ionosphere by low-altitude spacecraft [e.g., *Bonnell et al.*, 1996; *Wahlund et al.*, 1998] and are often associated with suprathermal electron bursts [e.g., *Knudsen et al.*, 1998; *Stasiewicz et al.*, 2000]. A variety of mechanisms for BB-ELF have been proposed, e.g., Alfven wave decay [e.g., *Wahlund et al.*, 1994; *Seyler et al.*, 1998], field-aligned electron current-driven instability [e.g., *Kintner et al.*, 1996; *Petkaki et al.*, 2003; *Petkaki and Freeman*, 2008], two-species ion-ion two-stream instability [e.g., *Gary and Omidi*, 1987; *Wahlund et al.*, 1992a], and transverse gradients in field-parallel plasma flow [e.g., *Gavrishchaka et al.*, 1999]. We focus on the current-driven mechanism as probably the most appropriate for the observations described below. This occurs when the electron velocity relative to the ions exceeds some threshold, and the plasma becomes unstable (e.g., electron-ion two-stream instability), and the instability then grows at the expense of the electron kinetic energy. Anomalous resistivity is a nonlinear function of the electron drift relative to the ions [*Petkaki and Freeman*, 2008]. This process can occur in a quasi-collisionless plasma such as the topside ionosphere, and the ion motion is not affected due to their higher mass [*Schunk and Nagy*, 2000]. The net additional electron "collision" process increases momentum loss and so creates additional "anomalous" resistivity. For ions and electrons drifting together, the resulting charge separation generates a field-aligned electric field, i.e., the anomalous electric field (E^*). Low-frequency ion density fluctuations are produced nonlinearly by precipitating electrons in auroral plasmas and can enhance the resistivity along the magnetic field line by several orders of magnitude over the ordinary collisional value [*Papadopoulos and Coffey*, 1974].

Natural ion upflow from the topside ionosphere is associated with either frictional heating and ion temperature enhancements (Type 1) or electron temperature enhancements (Type 2) [*Wahlund et al.*, 1992b]. The mechanism for Type 1 events appears to be enhanced ion pressure gradient accelerating the ions upward against gravity. For Type 2 events, *Wahlund et al.* [1992b] suggested that the mechanism is enhanced

*E** accelerating the ions upward against gravity, which is produced by anomalous resistivity due to plasma turbulence during particle precipitation events, i.e., above auroras. Using the electron energy balance equation, *Kagan and St. Maurice* [2005] showed this to be true for a single-case study. For ion upflow, *Wahlund et al.* [1993] estimated the anomalous electric field to be of order 1–10 μV/m.

Enhanced ion acoustic peaks in the incoherent scatter (IS) radar spectra, up to 1–2 orders of magnitude above normal [*Rietveld et al.*, 1991], are usually associated with intense *F* region red auroras [*Collis et al.*, 1991], indicating that high fluxes of low-energy precipitating electrons (less than a few hundred eV) were the cause of both phenomena. This situation is associated with electron heating and ion upflow [*Forme et al.*, 1995]. The larger the electron temperature is relative to the ion temperature the easier it is to produce enhanced ion acoustic electrostatic waves [*Kindel and Kennel*, 1971]. *Kindel and Kennel* [1971] showed that field-aligned currents, of typical amplitude associated with auroras [*Baumjohann*, 1982], were sufficient to stimulate both ion cyclotron and ion acoustic instabilities. However, *Rietveld et al.* [1991] showed that a low-flux beam of high-energy electrons would not produce an observable signature in the ion-line IS spectrum. They also identified the same low-flux beam of high-energy electrons as a likely generator mechanism for *E**.

The European Incoherent Scatter (EISCAT) facility in Tromsø, Norway (69.58°N, 19.22°E), includes a 930 MHz UHF IS radar [*Rishbeth and van Eyken*, 1993] colocated with a high-power high-frequency (HF) pump facility for artificial heating of the ionospheric plasma [*Rietveld et al.*, 1993]. The EISCAT radar spectra are analyzed using the grand unified incoherent scatter design and analysis package (GUISDAP) [*Lehtinen and Huuskonen*, 1996] to extract plasma density, ion and electron temperatures, and ion velocity as a function of range and time. Also colocated is the Digital All-Sky Imager (DASI-2), which consists of 1024 × 1024 pixels, thinned back-illuminated, high-quantum efficiency, cooled slow-scan charged-coupled device equipped with telecentric optics, and a six-position filter wheel.

It is well established that pumping the ionosphere with high-power HF radio waves causes plasma heating [e.g., *Robinson et al.*, 1996] with enhanced bulk electron temperatures up to 4000 K in the *F* region [e.g., *Rietveld et al.*, 2003]. These temperature enhancements may extend several hundred kilometers in altitude above the pump wave reflection height (typically ~200–250 km) [e.g., *Gustavsson et al.*, 2001, 2005] and sometimes beyond the typical maximum altitude observed by the EISCAT UHF radar (~600 km). Plasma heating may be accompanied by a significant flux of suprathermal electrons with sufficient energy to generate artificial optical emissions [*Kosch et al.*, 2007, and references therein] and to ionize the background gas [e.g., *Gustavsson et al.*, 2006]. Pump-induced electron energies can reach ~65 eV with typical optical emissions observed at 630, 557.7, and 844.6 nm with thresholds of ~2, 4.2, and 11 eV [*Gustavsson et al.*, 2005]. The intensity and spectrum of the optical emissions depend on the pump power [*Bryers et al.*, 2012], plasma resonance stimulated [*Bryers et al.*, 2013a], and pump frequency relative to the electron gyroharmonic frequency near the pump wave reflection altitude [*Kosch et al.*, 2002; *Gustavsson et al.*, 2006]. The pump-induced optical emissions may have a vertical extent exceeding ~200 km due to the flux of suprathermal electrons streaming up and down along the magnetic field line [*Pedersen et al.*, 2008]. The maximum altitude that optical emissions may be observed (~350 km) is limited by background neutral gas density, and the suprathermal electrons are expected to propagate higher in altitude.

Ionospheric pumping may result in the ion-line overshoot phenomenon in the IS spectrum near the pump wave reflection altitude [*Robinson*, 1989]. The ion-line backscatter power may increase by an order of magnitude or more. This is a well-known pump-induced Langmuir turbulence effect [*Djuth et al.*, 2004; *Rietveld et al.*, 2000] resulting in enhanced ion acoustic waves [e.g., *Kosch et al.*, 2010], which make normal analysis of the IS radar spectrum impossible. The phenomenon normally lasts less than 10 s but may become persistent when pumping near an electron gyroharmonic [*Honary et al.*, 1999]. However, ion-line overshoots generally only exist within a single radar range gate either side of the pump wave reflection altitude, i.e., a few kilometers.

In addition to electron heating, artificial ion upflows above ~400 km with upward field-aligned velocities up to ~300 m/s have also been reported by radar [e.g., *Rietveld et al.*, 2003; *Blagoveshchenskaya et al.*, 2005; *Kosch et al.*, 2010] and by in situ satellite [e.g., *Milikh et al.*, 2010; *Vartanyan et al.*, 2012] observations. *Kosch et al.* [2010] showed that the artificially induced electron pressure gradient enhancement could explain the phenomenon up to 600 km. The basic mechanism is that bulk electron heating alters the balance between the plasma pressure gradient and gravity, causing the electrons and ions to flow up along the magnetic field line together to conserve charge neutrality. The EISCAT radar observes the ion motion. A direct observation of the electron flow is not normally possible by IS radar.

With various simplifications suitable for the topside ionosphere [*Kosch et al*., 2010] the ion momentum equation describes the field-aligned motion of ions within a plasma:

$$\frac{\partial \vec{V}_{i||}}{\partial t} + \nu_{\text{in}}\left(\vec{V}_{i||} - \vec{V}_{n||}\right) = -\frac{1}{n_e m_i}\frac{\partial\left(n_e k_B\left(T_{i||} + T_{e||}\right)\right)}{\partial z} - \vec{g}_{||} \tag{1}$$

where V_i and V_n are the ion and neutral velocities, respectively, ν_{in} is the ion-neutral collision frequency, n_e is plasma density, m_i is ion mass, T_i and T_e are the ion and electron temperatures, respectively, g is gravity, k_B is Boltzmann's constant, t is time, and z is altitude. The right-hand side of equation (1) consists of the plasma pressure gradient, which is upward in the topside ionosphere, and gravity, which is downward. At high latitudes, it is generally reasonable to assume $V_{n||} = 0$ [*Aruliah and Rees*, 1995]. The magnitude of ν_{in} determines whether the force applied results primarily in ion acceleration or ion velocity. *Kosch et al*. [2010] found that up to ~450 km that ions moved with a quasi-constant velocity, and that the free acceleration regime was above the maximum observation altitude (600 km) of the radar. All terms in equation (1) can be observed experimentally, except for ν_{in}, which is derived.

For the topside ionosphere over EISCAT up to 600 km, the dominant ion is O^+. Below ~500 km, the dominant neutral is O. The resonant O–O^+ collision frequency is given by [*Schunk and Nagy*, 2000]:

$$\nu_{\text{in}}(\text{O} - \text{O}^+) = 3.67\times10^{-17} n_n(\text{O})\sqrt{T_{\text{in}}}(1 - 0.064\log_{10}T_{\text{in}})^2 \tag{2}$$

where n_n is the neutral density, and T_{in} is the average of the ion and neutral temperatures. Above ~500 km He must be taken into account. The nonresonant He–O^+ collision frequency is given by [*Schunk and Nagy*, 2000]:

$$\nu_{\text{in}}(\text{He} - \text{O}^+) = 1.32\times10^{-16} n_n(\text{He}) \tag{3}$$

For the case where E^* cannot be ignored, the ion momentum equation becomes

$$\sum \nu_{\text{in}}\vec{V}_{i||} = -\frac{1}{n_e m_i}\frac{\partial\left(n_e k_B\left(T_{i||} + T_{e||}\right)\right)}{\partial s} - \vec{g}_{||} + \frac{|e|}{m_i}\vec{E}^*_{||} \tag{4}$$

where $\Sigma\nu_{\text{in}}$ is the sum of all collision frequencies for all species, e is the charge of an electron, and we have assumed the steady state and $V_{n||} = 0$.

Using equations (1) and (2) for the above assumptions, *Vickers et al*. [2013] showed that the EISCAT Svalbard radar (ESR, 78.15°N, 16.02°E) [*Wannberg et al*., 1997] makes accurate estimates of the thermospheric neutral density for the unmodified ionosphere at 350 km and $Kp \leq 2$, which are also in good agreement with the Mass Spectrometer Incoherent Scatter (MSIS) model. These observations were verified by multiple in situ CHAMP drag observations when the satellite passed over the ESR. Equivalent observations have not yet been performed for the EISCAT UHF radar but we have no reason to expect a different outcome.

Kosch et al. [2010] used the modified ionosphere at EISCAT Tromsø to estimate thermospheric neutral density from equations (1) and (2). At 416 and 461 km altitudes, they found $n_n(\text{O}) = 1.29\times10^{14}\,\text{m}^{-3}$ and $1.03\times10^{14}\,\text{m}^{-3}$, which is 1.8 and 3.1 times greater than the MSIS model prediction, respectively. It is this discrepancy, which appears to increase with altitude, that is investigated in the present study. The difference suggests that another force is acting, which we take to be E^* as expressed in equation (4).

2. Experiment and Results

A complex ionospheric modification experiment was executed at EISCAT in the period from 22 October to 3 November 2013, using multiple pump frequencies, wave polarizations, and beam pointing directions. Much of this campaign has been described (N. Blagoveshchenskaya et al., Optical and ionospheric phenomena at EISCAT under continuous X-mode HF pumping, submitted to *Journal of Geophysical Research*, 2014).

We concern ourselves only with two pump pulses on 23 October 2013 at 17:01 and 17:31 UT where there was clear evidence of pump-induced ion upflow. These times correspond to a period of very low geomagnetic activity ($Kp = 0$). The pump beam at 6.2 MHz was pointing field aligned with an effective radiated power of ~550 MW, *O*-mode polarization, and a pump cycle of 5 min on, 2.5 min off. The pump frequency is far away from any electron gyroharmonic in the *F* region. The UHF radar was observing field aligned from 49 to 694 km using the 32×20 alternating "beata" code with 10 μs sampling, 1.5–3 km range resolution, and data time resolution of 5 s.

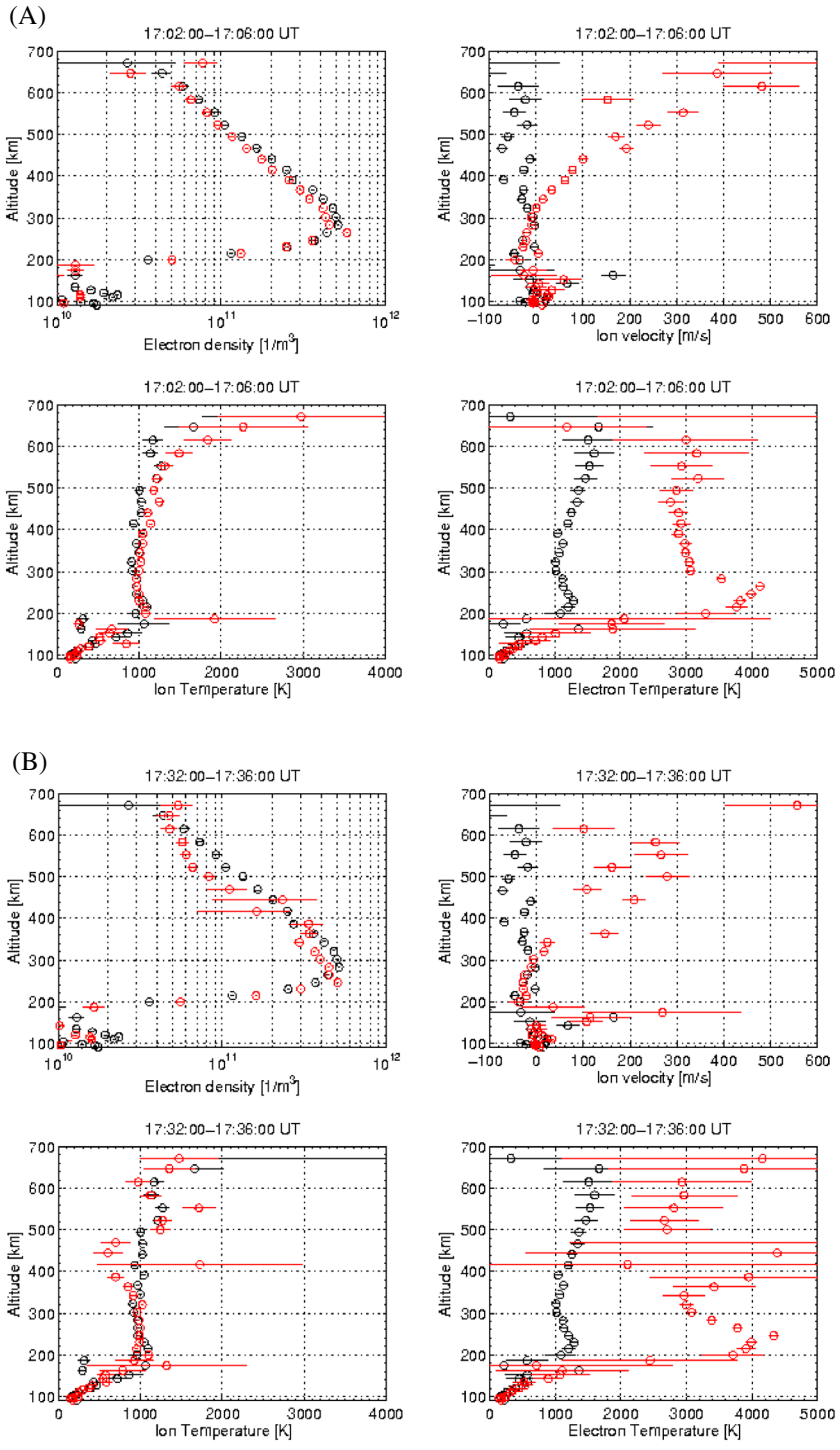

Figure 1. EISCAT field-aligned radar observations for 23 October 2013 for the selected intervals of (a) 17:02–17:06 and (b) 17:32–17:36 UT. Pump-on data are in red. Pump-off data (17:21–17:24 UT) are in black. Shown as a function of altitude are electron density (Figures 1a and 1b, top left), ion velocity (Figures 1a and 1b, top right), ion temperature (Figures 1a and 1b, bottom left), and electron temperature (Figures 1a and 1b, bottom right). The data uncertainty is also indicated.

We check the validity of our neutral wind assumption (i.e., $V_{n||} = 0$). Only the meridional neutral wind is important at EISCAT due to the near southward orientation of the local magnetic field (azimuth = 182°). The dip angle is 77.2°, so only strong horizontal winds will generate a significant field-aligned flow. Using over 8 years of Fabry-Perot interferometer data from northern Scandinavia, *Aruliah et al.* [1996] show that the

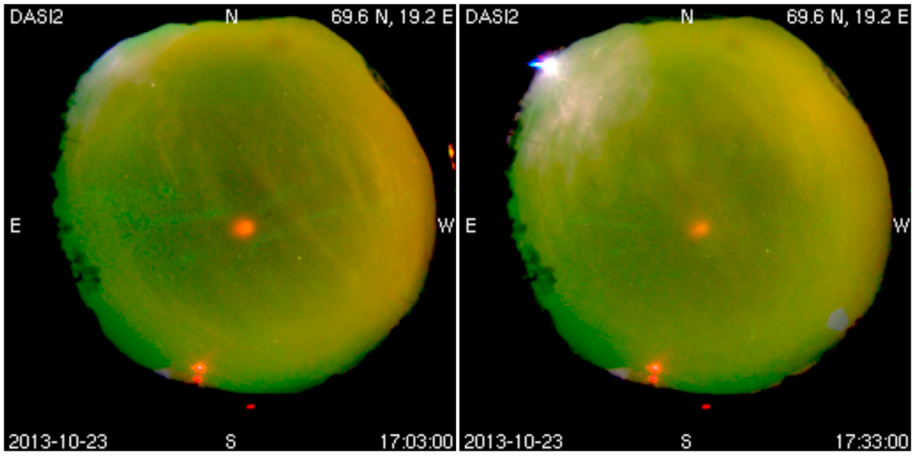

Figure 2. All-sky images for (left) 17:03 UT and (right) 17:33 UT.

meridional neutral wind is close to zero for our universal time, season, geomagnetic activity, and solar cycle phase. Hence, this variable is ignored. Regarding the steady state assumption, pump-induced ionospheric effects in the *F* region normally stabilize within less than 1 min [cf. *Gustavsson et al.*, 2001]. Hence, we only integrate the final 4 min of both 5 min pump pulses, i.e., 17:02–06 and 17:32–36 UT.

Figures 1a and 1b show the EISCAT radar data at 17:02–17:06 and 17:32–17:36 UT, respectively, on 23 October 2013 for pump on in red. Background data from the pump-off period 17:21–17:24 UT is shown in black. Figures 1a and 1b (top left) show electron density, which is essentially unperturbed by the pump wave. The variation in plasma density is due to natural causes. The ionosphere is over dense at 6.2 MHz with the HF reflection height estimated at 255 and 243 km for 17:01 and 17:31 UT, respectively. Figures 1a and 1b (top right) show field-aligned ion velocity, which is enhanced by the pump action and positive (upward) above 300 km altitude. Above ~400 km, ion upflow of ~100–300 km/s is observed, with ions accelerating to higher velocities at higher altitudes as expected from equation (1). Below 280 km the ion velocity is negative (downward) with velocities up to ~40 m/s. The smaller downward velocities are consistent with observations of naturally induced ion flow [*Buchert et al.*, 2004]. The background data (black) shows negative (downward) ion motion up to ~80 m/s, as is expected between pump-on periods. Figures 1a and 1b (bottom left) show the ion temperature, which is essentially unperturbed by the pump wave. Figures 1a and 1b (bottom right) show the electron temperature, with enhanced values up to ~4000 K above ~200 km. The greatest temperature enhancements occur at the pump wave reflection altitude, with the hot electrons streaming up and down the magnetic field line.

Intense pump-induced optical emissions were observed during this experiment by the DASI-2. Observations at 630, 557.7, and 844.6 nm were made using 3, 8, and 13 s integration, respectively, in a 30 s cycle. Example pseudo-real color images are shown in Figure 2 for 17:03 and 17:33 UT. The red blob near the middle of the images is the pump-induced optical emission, dominated by 630 nm, located on the magnetic field line connected to EISCAT. The red illumination near the southern horizon is aircraft warning lights on a nearby tower. The green and yellow colors within the images indicate natural aurora and clouds reflecting sodium street lighting, respectively. The pump-induced optical emissions are a clear indication of suprathermal electrons from wave-plasma resonance near the HF reflection altitude [*Bryers et al.*, 2013b].

Unfortunately, the optical data are contaminated by drifting clouds on 23 October 2013, making an intensity estimate a minimum value. Also, for the pump pulse of 17:31 UT, there is contamination by the moon, seen on the northeast horizon. The optical emission intensities were at least 1910, 370, and 100 R for 630, 557.7, and 844.6 nm, respectively, for the pump pulse at 17:01 UT, and 1150, 170, and 100 R for 630, 557.7, and 844.6 nm, respectively, for the pump pulse at 17:31 UT. These values are certainly among the most intense ever observed at EISCAT [cf. *Kosch et al.*, 2007] and a clear indication of a significant flux of pump-induced suprathermal electrons exceeding 11 eV [*Bryers et al.*, 2013b].

Table 1 shows results for the two pump pulses (17:02 and 17:32 UT) using 4 min integration of the EISCAT data in the steady state for three altitudes (390, 495, and 580 km) corresponding to closest available radar range gates where ion upflow was significant. The first column shows time. The second column shows the

Table 1. For Three Different Altitudes, the First Column Shows the Pump Pulse Steady State Start Time, the Second Column Shows the Radar Estimate of Atomic Oxygen Density With Percentage Uncertainty, the Third and Fourth Columns Show the MSIS Model Prediction of Atomic Oxygen and Helium Density, and the Fifth Column Shows the Estimated Anomalous Electric Field With Percentage Uncertainty

UT	EISCAT n(O)/m^3	MSIS n(O)/m^3	MSIS n(He)/m^3	E^* V/m
		Altitude: *390 km*		
17:02	1.66E+14 ± 10%	1.30E+14	6.21E+12	−2.33E−6 ± 10.4%
17:32	1.48E+14 ± 10.7%	1.30E+14	6.21E+12	−2.38E−6 ± 11.3%
		Altitude: *495 km*		
17:02	1.80E+13 ± 13.1%	2.32E+13	4.03E+12	−9.18E−7 ± 20.5%
17:32	7.10E+13 ± 16.9%	2.32E+13	4.03E+12	−2.69E−6 ± 15.8%
		Altitude: *580 km*		
17:02	1.39E+13 ± 42.7%	5.53E+12	2.82E+12	−4.04E−7 ± 95.8%
17:32	2.43E+13 ± 33.1%	5.53E+12	2.82E+12	−9.73E−7 ± 55.0%

estimated neutral atomic oxygen density, using equations (1) and (2). The third column shows the MSIS model prediction of atomic oxygen density. EISCAT overestimates the neutral density, increasingly so with altitude, using the simplified ion momentum equation. The percentage difference on average is 20.8% at 390 km, 91.8% at 495 km, and 245.4% at 580 km. This is consistent with the observation made by *Kosch et al*. [2010]. The fourth column shows the MSIS model prediction for atomic helium density. This is a relative minor species at 390 and 495 km but becomes significant at 580 km. The fourth column shows the value of E^* required to satisfy equation (4) where MSIS has been used as the input in equations (2) and (3). The basis upon which MSIS densities are accepted as correct is the good agreement with the ESR and CHAMP satellite conjunctions at ~350 km [*Vickers et al*., 2013]. E^* always points downward and varies in amplitude from ~0.4 to 2.4 μV/m, weakening with increasing altitude. This is consistent with *Wahlund et al*. [1993]. The estimated uncertainties are shown as percentages, propagated from the GUISDAP analysis of the radar spectra. The uncertainty increases with altitude as the radar signal decreases.

3. Discussion

Our hypothesis is as follows: The HF pump wave produces a plasma resonance in the bottom-side ionosphere, in our case around 243 and 255 km. This causes electron heating of the bulk thermalized plasma up to 4000 K (see Figure 1), as observed by the EISCAT radar, as well as accelerating a small but significant flux of suprathermal electrons to energies up to at least 11 eV, as observed by the artificially induced optical emissions (see Figure 2). Previous side-viewing observations of pump-induced optical emissions show they appear up to 100–200 km in height extent [*Gustavsson et al*., 2008; *Pedersen et al*., 2008], showing that the suprathermal electrons propagate upward from the plasma resonance region and therefore constitute a downward current in the topside ionosphere. How rapidly the pump-induced suprathermal electrons propagate up the magnetic field line has never been observed experimentally because the low cadence of the imagers. However, the observed optical emissions with threshold energies >2 eV suggest a linear electron velocity of order 10^6 m/s, which is about an order of magnitude greater than the critical electron velocity required to stimulate ion acoustic waves [*Petkaki et al*., 2003] and therefore seed the mechanism for anomalous resistivity [cf. *Mishin and Khazanov*, 2006]. No evidence of these ion acoustic waves appears in the radar spectra, as expected by *Rietveld et al*. [1991].

The heated bulk electron plasma increases the plasma pressure gradient, overcoming the balance with gravity in the topside ionosphere, so causing bulk electron and ion upflow and downflow above and below the *F* region electron density peak (~280 km), respectively, as observed by the EISCAT radar (see Figure 1). These charges move together, so no current results. The ions are unaffected by the anomalous resistivity. However, the bulk thermalized electrons are scattered and retarded, causing a small charge separation. The electrons will lag the ions, resulting in a downward electric field in the topside ionosphere, as we have estimated (see Table 1). The direction of the anomalous electric field is opposite to that expected for the natural case because the field-aligned current generated by the pump-induced suprathermal electron flux is in the opposite direction compared to auroras.

Qualitatively, the hypothesis seems clear. Unfortunately, IS radar does not normally observe the electron velocity or field-aligned current. We make a simple estimate of the current carried by the suprathermal

electrons and from this the anomalous resistivity. The 630 nm optical emissions (I_{6300}) were at least 1150 and 1910 R for the two pump pulses analyzed, with an average of 1530 R ($I_{6300} = 1.53 \times 10^{10}$ ph m^{-2} s^{-1}). For a different experiment, *Gustavsson et al*. [2008] estimated that the full width at half maximum (FWHM) optical intensity was ~ ±24.5 km, assuming a Gaussian distribution, around a peak altitude of 204 km, accounting for 80.3% of the photon production volume. No side-viewing optical data were available on 23 October 2013 due to clouds, but such data from 22 October 2013 are consistent with the optical FWHM estimate albeit at a higher altitude of ~225 km (Figure 2 of N. Blagoveshchenskaya, submitted manuscript, 2014). We estimate the O(^{1}D) excitation rate (q) from $q = I_{6300}/(A_{6300}\tau_{ave})$ [*Gustavsson et al*., 2001], where $A_{6300} = 5.15 \times 10^{-3}$ s^{-1} is the Einstein coefficient and τ_{ave} is the altitude-dependent O(^{1}D) effective lifetime. For ~225–250 km, $\tau_{ave} \approx 20$ s [*Gustavsson et al*., 2001], giving $q = 1.49 \times 10^{11}$ m^{-2} s^{-1}.

Hysell et al. [2012] found that the suprathermal electron flux had a broad peak around 5 eV. We now assume that the mean energy of the suprathermal electrons is 5 eV. This is close to the peak (~6 eV) in the O(^{1}D) collision cross-section (σ) profile [*Gustavsson et al*., 2005] with $\sigma \approx 4 \times 10^{-21}$ m^{-2} [*Gustavsson et al*., 2005]. The inelastic collision frequency (ν) with atomic oxygen is $\nu = v_e \sigma n(\mathrm{O})$, where v_e is the electron velocity and n(O) is the atomic oxygen density. For our height range and selected energy, $\nu(\mathrm{O}(^1\mathrm{D})) = 1.27 \times 10^6 \times 4 \times 10^{-21} \times 3.12 \times 10^{15} = 16$ Hz. The mean free path (λ) is $\lambda = 1/(\sigma n(\mathrm{O}))$. We ignore N_2 and N_2^+ since their collision cross sections are negligible at 5 eV or less. Hence, $\lambda = 80.1$ km. If the FWHM of the optical emission is ~49 km, this suggests that approximately 49/80.1 = 61.2% of suprathermal electron streaming out from the HF reflection height will produce an excited O(^{1}D) state, which eventually produces an observable photon.

Assuming that half the suprathermal electrons stream up and down the magnetic field line away from the HF reflection altitude, the current must be at least $0.5 \times 1.6 \times 10^{-19} \times 1.49 \times 10^{11}/0.612 = 1.94 \times 10^{-8}$ A/m^2. Taking into account the other excited states resulting in other optical emissions, *Bryers et al*. [2012] estimated that about one third of the suprathermal electron flux would account for the 630 nm emission. Hence, the estimated minimum current is about 5.82×10^{-8} A/m^2. The average anomalous electric field we have observed at 390 and 495 km is 2.36 and 1.8 μV/m, giving an anomalous resistivity (η^*) of $2.36 \times 10^{-6}/5.82 \times 10^{-8} = 40.55$ and $1.8 \times 10^{-6}/5.82 \times 10^{-8} = 30.92$ Ωm, respectively. The estimated ionospheric collisional resistivity at 390 and 495 km is 3.7×10^{-2} and 8.6×10^{-2} Ωm [e.g., *Hargreaves*, 1992], making our simple estimate of anomalous resistivity 1096 and 360 times greater, respectively. This is in the range (10^2–10^4) predicted by *Papadopoulos and Coffey* [1974].

The suprathermal electron elastic collision frequency is at least an order of magnitude greater than for the atomic oxygen nonelastic collisions. Since elastic collisions tend to make the electron flux more isotropic, and the source region of the suprathermal electrons (HF reflection altitude) is above the region of maximum photon production (because the oxygen density is greater at lower altitudes), it is expected that the number of suprathermal electrons reflected back up the magnetic field line from below the HF reflection altitude will be greater than those reflected down from above the HF reflection altitude. This follows quite simply from the fact that the neutral density is declining exponentially with increasing altitude. Hence, due to this imbalance, the upward flux of suprathermal electrons will be greater than our simple estimate, thereby reinforcing our analysis.

A question arises as to why enhanced low-frequency ion acoustic waves leading to anomalous resistivity are not routinely observed by the IS radar during ionospheric pumping experiments. *Senior et al*. [2013] did report observing plasma density enhancements over a height range of ~125 km during an ionospheric pumping experiment, and this may be a signature of ion acoustic waves. However, we note that auroral precipitation routinely produces anomalous resistivity during natural auroras without any obvious signature of enhanced ion acoustic waves in the EISCAT radar spectra.

A weakness of this experiment for our purpose were the short pump-off periods, which do not allow enough time for adequate radar data integration during the steady state. Hence, we have not been able to estimate E^* during the pump-off periods with confidence.

4. Conclusion

We have inferred the anomalous electric field in the topside ionosphere (390–580 km) using the EISCAT ionospheric modification facility and UHF radar, and applying the modified ion momentum equation in the steady state with the MSIS model. When pumping the ionosphere with high-power HF radio waves,

the bulk electron temperature is significantly raised, increasing the plasma pressure gradient in the topside ionosphere, which results in ion upflow along the magnetic field line. Using EISCAT radar data, the modified ion momentum equation in the steady state and the MSIS model, the anomalous field-aligned electric field was estimated. From the pump-induced optical emissions and MSIS model, the suprathermal electron flux, field-aligned current, and anomalous resistivity were estimated. For our data in the steady state, the anomalous electric field points downward with average amplitude of ~1.6 μV/m, and we estimate the anomalous resistivity to be 2 to 3 orders of magnitude greater than the collisional resistivity, both of which are consistent with previous work. The seed for the anomalous resistivity is thought to be the suprathermal flux of pump-induced energetic electrons, which are generated near the pump wave reflection altitude by wave-plasma resonance and which also produce artificially induced auroral optical emissions.

Acknowledgments

EISCAT is an international association supported by research organizations in China (CRIRP), Finland (SA), Japan (NIPR and STEL), Norway (NFR), Sweden (VR), and the United Kingdom (NERC). M.J.K. was supported by the National Institute for Polar Research in the form of a visiting professorship. The production of this paper was supported by a NIPR publication subsidy. The EISCAT data used in this paper are available through the Madrigal database (http://www.eiscat.se/madrigal/). The optical data are available from M.J.K. or A.S.

W. K. Peterson thanks Jan-Erik Wahlund and Evgeny Mishin for their assistance in evaluating this paper.

References

Aruliah, A. L., and D. Rees (1995), The trouble with thermospheric vertical winds: Geomagnetic, seasonal and solar cycle dependence at high latitudes, *J. Atmos. Sol. Terr. Phys.*, *57*, 597–609.

Aruliah, A. L., A. D. Farmer, D. Rees, and U. Brändström (1996), The seasonal behavior of high-latitude thermospheric winds and ion velocities observed over one solar cycle, *J. Geophys. Res.*, *101*, 15,701–15,711, doi:10.1029/96JA00360.

Baumjohann, W. (1982), Ionospheric and field-aligned current systems in the auroral zone: A concise review, *Adv. Space Res.*, *2*, 55–62.

Blagoveshchenskaya, N. F., V. A. Kornienko, T. D. Borisova, M. T. Rietveld, T. Bösinger, B. Thide, T. B. Leyser, and A. Brekke (2005), Heater-induced phenomena in a coupled ionosphere-magnetosphere system, *Adv. Space Res.*, *38*, 2495–2502.

Bonnell, J., P. Kintner, J.-E. Wahlund, K. Lynch, and R. Arnoldy (1996), Interferometric determination of broadband ELF wave phase velocity within a region of transverse auroral ion acceleration, *Geophys. Res. Let.*, *23*, 3297–3300.

Bryers, C. J., M. J. Kosch, A. Senior, M. T. Rietveld, and T. K. Yeoman (2012), EISCAT observations of pump-enhanced plasma temperature and optical emission excitation rate as a function of power flux, *J. Geophys. Res.*, *117*, A09301, doi:10.1029/2012JA017897.

Bryers, C. J., M. J. Kosch, A. Senior, M. T. Rietveld, and T. K. Yeoman (2013a), The threshold of plasma instabilities pumped by high frequency radio waves at EISCAT, *J. Geophys. Res. Space Physics*, *118*, 7472–7481, doi:10.1002/2013JA019429.

Bryers, C. J., M. J. Kosch, A. Senior, M. T. Rietveld, and W. Singer (2013b), A comparison between resonant and non-resonant heating at EISCAT, *J. Geophys. Res. Space Physics*, *118*, 6766–6776, doi:10.1002/jgra.50605.

Buchert, S. C., Y. Ogawa, R. Fujii, and A. P. van Eyken (2004), Observations of diverging field-aligned ion flow with the ESR, *Ann. Geophys.*, *22*, 889–899.

Collis, P. N., I. Häggström, K. Kaila, and M. T. Rietveld (1991), EISCAT radar observations of enhanced incoherent scatter spectra: Their relation to red aurora and field-aligned currents, *Geophys. Res. Lett.*, *18*, 1031–1034, doi:10.1029/91GL00848.

Djuth, F. T., B. Isham, M. T. Rietveld, T. Hagfors, and C. La Hoz (2004), The first one hundred milliseconds of HF modification at Tromsø, Norway, *J. Geophys. Res.*, *109*, A11307, doi:10.1029/2003JA010236.

Forme, F. R. E., D. Fontaine, and J. E. Wahlund (1995), Two different types of enhanced ion acoustic fluctuations observed in the upper ionosphere, *J. Geophys. Res.*, *100*, 14,625–14,636, doi:10.1029/94JA01093.

Gary, S. P., and N. Omidi (1987), The ion-ion acoustic instability, *J. Plasma Phys.*, *37*, 45–61.

Gavrishchaka, V. V., S. B. Ganguli, and G. I. Ganguli (1999), Electrostatic oscillations due to filamentary structures in the magnetic-field-aligned flow: The ion-acoustic branch, *J. Geophys. Res.*, *104*, 12,683–12,693, doi:10.1029/1999JA900094.

Gustavsson, B., et al. (2001), First tomographic estimate of volume distribution of HF pump enhanced airglow emission, *J. Geophys. Res.*, *106*, 29,105–29,124, doi:10.1029/2000JA900167.

Gustavsson, B., et al. (2005), The electron distribution during HF pumping, a picture painted with all colors, *Ann. Geophys.*, *23*(5), 1747–1754.

Gustavsson, B., T. B. Leyser, M. J. Kosch, M. T. Rietveld, A. Steen, B. U. E. Brändström, and T. Aso (2006), Electron gyroharmonic effects in ionization and electron acceleration during HF pumping in the ionosphere, *Phys. Rev. Lett.*, *97*, 195002, doi:10.1103/PhysRevLett.97.195002.

Gustavsson, B., M. Kosch, A. Wong, T. Pedersen, C. Heinselman, C. Mutiso, B. Bristow, J. Hughes, K. Nielsen, and W. Wang (2008), First estimates of altitude distribution of HF-pump enhanced emissions at 6300 and 5577 A: A comparison between observations and theory, *Ann. Geophys.*, *26*, 3999–4012.

Hargreaves, J. K. (1992), *The Solar-Terrestrial Environment*, Cambridge Univ. Press, Cambridge, U. K.

Honary, F., T. R. Robinson, D. M. Wright, A. J. Stocker, M. T. Rietveld, and I. McCrea (1999), First direct observations of the reduced striations at pump frequencies close to the electron gyroharmonics, *Ann. Geophys.*, *17*, 1235–1238.

Hysell, D. L., R. H. Varney, M. N. Vlasov, E. Nossa, B. Watkins, T. Pedersen, and J. D. Huba (2012), Estimating the electron energy distribution during ionospheric modification from spectrographic airglow measurements, *J. Geophys. Res.*, *117*, A02317, doi:10.1029/2011JA017187.

Kagan, L. M., and J.-P. St. Maurice (2005), Origin of type-2 thermal-ion upflows in the auroral ionosphere, *Ann. Geophys.*, *23*, 13–24.

Kindel, J. M., and C. F. Kennel (1971), Topside current instabilities, *J. Geophys. Res.*, *76*, 3055–3078, doi:10.1029/JA076i013p03055.

Kintner, P. M., J. Bonnell, R. Arnoldy, K. Lynch, C. Pollock, and T. Moore (1996), SCIFER—Transverse ion acceleration and plasma waves, *Geophys. Res. Lett.*, *23*, 1873–1876, doi:10.1029/96GL01863.

Knudsen, D. J., J. H. Clemmons, and J.-E. Wahlund (1998), Correlation between core ion energization, suprathermal electron bursts, and broadband ELF plasma waves, *J. Geophys. Res.*, *103*, 4171–4186, doi:10.1029/97JA00696.

Kosch, M. J., M. T. Rietveld, A. J. Kavanagh, C. Davis, T. Yeoman, F. Honary, and T. Hagfors (2002), High-latitude pump-induced optical emissions for frequencies close to the third electron gyro-harmonic, *Geophys. Res. Lett.*, *29*(23), 2112–2115, doi:10.1029/2002GL015744.

Kosch, M. J., T. Pedersen, M. T. Rietveld, B. Gustavsson, S. M. Grach, and T. Hagfors (2007), Artificial optical emissions in the thermosphere induced by powerful radio waves: An observational review, *Adv. Space Res.*, *40*(3), 365–376.

Kosch, M. J., Y. Ogawa, M. T. Rietveld, S. Nozawa, and R. Fujii (2010), An analysis of pump-induced artificial ionospheric ion upwelling at EISCAT, *J. Geophys. Res.*, *115*, A12317, doi:10.1029/2010JA015854.

Lehtinen, M. S., and A. Huuskonen (1996), General incoherent scatter analysis and GUISDAP, *J. Atmos. Sol.-Terr. Phys.*, *58*, 435–452, doi:10.1016/0021-9169(95)00047-X.

Milikh, G. M., E. Mishin, I. Galkin, A. Vartanyan, C. Roth, and B. W. Reinisch (2010), Ion outflows and artificial ducts in the topside ionosphere at HAARP, *Geophys. Res. Lett.*, *37*, L18102, doi:10.1029/2010GL044636.

Mishin, E. V., and G. V. Khazanov (2006), Tether-induced airglow: Collisionless effects, *Geophys. Res. Lett.*, *33*, L15105, doi:10.1029/2006GL026220.

Papadopoulos, K. (1977), A review of anomalous resistivity for the ionosphere, *Rev. Geophys. Space Phys.*, *15*, 113–127.

Papadopoulos, K., and T. Coffey (1974), Anomalous resistivity in the auroral plasma, *J. Geophys. Res.*, *79*, 1558–1561, doi:10.1029/JA079i010p01558.

Pedersen, T., R. J. Esposito, E. A. Kendall, D. Sentman, M. Kosch, E. V. Mishin, and R. A. Marshall (2008), Observations of artificial and natural optical emissions at the HAARP facility, *Ann. Geophys.*, *26*(5), 1089–1099.

Petkaki, P., and M. P. Freeman (2008), Nonlinear dependence of anomalous ion-acoustic resistivity on electron drift velocity, *Astrophys. J.*, *686*(1), 686–693.

Petkaki, P., C. E. J. Watt, R. B. Horne, and M. P. Freeman (2003), Anomalous resistivity in non-Maxwellian plasmas, *J. Geophys. Res.*, *108*(A12), 1442, doi:10.1029/2003JA010092.

Rietveld, M. T., P. N. Collis, and J.-P. St.-Maurice (1991), Naturally enhanced ion acoustic waves in the auroral ionosphere observed with the EISCAT 933-MHz radar, *J. Geophys. Res.*, *96*, 19,291–19,305, doi:10.1029/91JA01188.

Rietveld, M. T., H. Kohl, H. Kopka, and P. Stubbe (1993), Introduction to ionospheric heating at Tromso I—Experimental overview, *J. Atmos. Terr. Phys.*, *55*, 577–599.

Rietveld, M. T., B. Isham, H. Kohl, C. La Hoz, and T. Hagfors (2000), Measurements of HF-enhanced plasma and ion lines at EISCAT with high altitude resolution, *J. Geophys. Res.*, *105*(A4), 7429–7439, doi:10.1029/1999JA900476.

Rietveld, M. T., M. J. Kosch, N. R. Blagoveshchenskaya, V. A. Kornienko, T. B. Leyser, and T. K. Yeoman (2003), Ionospheric electron heating, optical emissions and striations induced by powerful HF radio waves at high latitudes: Aspect angle dependence, *J. Geophys. Res.*, *108*(A4), 1141, doi:10.1029/2002JA009543.

Rishbeth, H., and A. P. van Eyken (1993), EISCAT: Early history and the first ten years of operation, *J. Atmos. Terr. Phys.*, *55*, 525–542.

Robinson, T. R. (1989), The heating of the high latitude ionosphere by high power radio waves, *Physics Rep.*, *179*, 79–209.

Robinson, T. R., F. Honary, A. J. Stocker, T. B. Jones, and P. Stubbe (1996), First EISCAT observations of the modification of F-region electron temperatures during RF heating at harmonics of the electron gyro frequency, *J. Atmos. Terr. Phys.*, *58*, 385–395.

Schunk, R. W., and A. F. Nagy (2000), *Ionospheres: Physics, Plasma Physics, and Chemistry*, Cambridge Univ. Press, New York.

Senior, A., M. T. Rietveld, I. Haggstrom, and M. J. Kosch (2013), Radio-induced incoherent scatter ion line enhancements with wide altitude extents in the high-latitude ionosphere, *Geophys. Res. Lett.*, *40*, 1669–1674, doi:10.1002/grl.50272.

Seyler, C. E., A. E. Clark, J. Bonnell, and J.-E. Wahlund (1998), Electrostatic broadband ELF wave emission by Alfvén wave breaking, *J. Geophys. Res.*, *103*, 7027–7041, doi:10.1029/97JA02297.

Stasiewicz, K., et al. (2000), Small scale Alfvénic structure in the aurora, *Space Sci. Rev.*, *92*, 423–533.

Vartanyan, A., G. M. Milikh, E. Mishin, M. Parrot, I. Galkin, B. Reinisch, J. Huba, G. Joyce, and K. Papadopoulos (2012), Artificial ducts caused by HF heating of the ionosphere by HAARP, *J. Geophys. Res.*, *117*, A10307, doi:10.1029/2012JA017563.

Vickers, H., M. J. Kosch, E. Sutton, Y. Ogawa, and C. LaHoz (2013), Thermospheric atomic oxygen density estimates using the EISCAT Svalbard Radar, *J. Geophys. Res. Space Physics*, *118*, 1319–1330, doi:10.1002/jgra.50169.

Wahlund, J.-E., F. R. E. Forme, H. J. Opgenoorth, M. A. L. Persson, E. V. Mishin, and A. S. Volokitin (1992a), Scattering of electromagnetic waves from a plasma: Enhanced ion acoustic fluctuations due to ion-ion two-stream instabilities, *Geophys. Res. Lett.*, *19*, 1919–1922, doi:10.1029/92GL02101.

Wahlund, J.-E., H. J. Opgenoorth, I. Häggström, K. J. Winser, and G. O. L. Jones (1992b), EISCAT observations of strong ion outflows from the F-region ionosphere during auroral activity: Revisited, *J. Geophys. Res.*, *97*, 3019–3037, doi:10.1029/91JA02438.

Wahlund, J.-E., H. J. Opgenoorth, F. R. E. Forme, M. A. L. Persson, I. Häggström, and J. Lilensten (1993), Electron energization in the topside auroral ionosphere: On the importance of ion-acoustic turbulence, *J. Atmos. Terr. Phys.*, *55*, 623–645.

Wahlund, J.-E., P. Louarn, T. Chust, H. De Feraudy, A. Roux, B. Holback, P.-O. Dovner, and G. Holmgren (1994), On ion acoustic turbulence and the nonlinear evolution of kinetic Alfven waves in aurora, *Geophys. Res. Lett.*, *21*, 1831–1834, doi:10.1029/94GL01289.

Wahlund, J.-E., et al. (1998), Broadband ELF plasma emission during auroral energization: 1. Slow ion acoustic waves, *J. Geophys. Res.*, *103*, 4343–4375, doi:10.1029/97JA02008.

Wannberg, G., et al. (1997), The EISCAT Svalbard Radar: A case study in modern incoherent scatter radar system design, *Radio Sci.*, *32*(6), 2283–2307, doi:10.1029/97RS01803.